Mechanical Systems and Signal Processing 161 (2021) 107991

Contents lists available at ScienceDirect

Mechanical Systems and Signal Processing

journal homepage: www.elsevier.com/locate/ymssp

An approach to the solution of nonlinear forced vibration problem of structural systems reinforced with advanced materials in the presence of viscous damping

A.H. Sofiyev [a,*], M. Avey [b], N. Kuruoglu [c]

[a] Department of Civil Engineering of Engineering Faculty of Suleyman, Demirel University, Isparta, Turkey
[b] Division of Mathematics in Graduate School of Natural and Applied Sciences of Usak University, Usak, Turkey
[c] Department of Civil Engineering of Faculty of Engineering and Architecture, Istanbul Gelisim University, Istanbul, Turkey

ARTICLE INFO

Handling Editor: Xingjian Jing

Keywords:
Nonlinear forced vibration
CNTs
Structural systems
Multi-scales method
External excitation
Viscous damping

ABSTRACT

In this study, the nonlinear forced vibration of composite structural systems such as plates, panels and shells reinforced with advanced materials in the presence of linear viscous damping is investigated. Hamilton principle and von Kármán-type nonlinear theory are used to obtain the theoretical model of double-curved shells reinforced by carbon nanotubes (CNTs). The nonlinear partial differential equations are reduced to ordinary differential equations using Galerkin method. By using the multiscale method, the frequency-amplitude relation and nonlinear forced vibration frequency of structural systems are obtained for the first time. Since double-curved shells can be transformed into other structural systems such as spherical and hyperbolic-paraboloid shells, rectangular plate and cylindrical panel in special cases, the expressions for nonlinear frequencies can also be used for them. In additional, the backbone curve and the nonlinear frequency/linear frequency ratio are determined as a function of the amplitude in primary resonance for the first time. The results are verified by comparing the reliability and accuracy of the proposed formulation with those in the literature. Finally, a systematic study is aimed at controlling the influence of nonlinearity and types of distribution of CNTs on the frequencies and their quantitative and qualitative variation in the presence of external excitation and viscous damping.

1. Introduction

In most aerospace applications, structural systems such as plates, panels, and shells serve as coating elements in a rocket system and are also used as part of a sealed fuel tank. The many stringent requirements for structural systems have led to the rapid development of two areas: new materials technologies and more sophisticated analytical methods. Recent developments in materials technology have moved away from traditional materials, and new composite materials reinforced with carbon nanotubes are preferred to meet the stringent requirements of more efficient and lighter vehicles. In this sense, the discovery of carbon nanotubes (CNT) by Iijima in 1991 became a turning point in many practical areas of nanotechnology and led to their wide application [1]. Single-walled carbon nanotubes (SWNTs) in the form of hollow long cylindrical pipes consist of an atomic carbon layer in the honeycomb cage, and when its

* Corresponding author at: Department of Civil Engineering of Engineering Faculty, Suleyman Demirel University, 32260 Isparta, Turkey.
E-mail address: abdullahavey@sdu.edu.tr (A.H. Sofiyev).

https://doi.org/10.1016/j.ymssp.2021.107991
Received 21 March 2021; Received in revised form 14 April 2021; Accepted 21 April 2021
Available online 8 May 2021

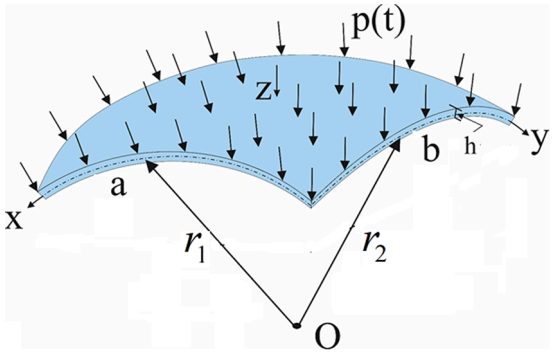

Fig. 1. The double-curved shell reinforced by CNTs.

diameter is in the nanometer range, its length can even exceed centimeters. More details about CNT features are included in the work of Shaffer and Windle [2]. Ajayan et al. [3] provided a simple method to produce aligned carbon nanotube arrays in its study, allowing composites reinforced by CNTs to be applied to various engineering disciplines. SWCNTs are often used as reinforcing particles in the production of CNTRCs. The composites reinforced by CNTs are widely used in many fields, including mechanical, aerospace, civil and biomedical, as forming materials for beams, plates and shell-like structures [4]. There are notable studies in the literature on structural modeling, the production of composites reinforced by CNTs, and the determination of material properties of polymer matrix reinforced by CNTs using MD simulations [5–10].

The forced vibrations are not damped, unlike natural vibrations. Under certain conditions, such vibrations can be very dangerous for real structural elements, since the amplitude of the vibrations, as well as the stresses and strains in the shells, increase dramatically. Even when stresses are within elastic limits, the forced vibrations can cause fatigue cracks to form, leaving the structure unusable. The problem of studying steady-state forced vibrations is relevant for structures used for various purposes, due to the wide application in practice of loading modes, which cause intense resonant vibrations in them. The study of forced vibration of structural systems in the finite deflections is very important for the design of aviation structures, as shown in references [11–30].

The idea of functionally graded materials (FGMs) was proposed in the study of Suresh and Mortensen [31] to alleviate the problem of weak interfacial bonding between CNTs and polymers, so that CNT-based composite structures have a smooth and continuous variation in an isotropic matrix in the desired direction and this idea was realized in the study of Shen [32]. The use of structural elements made of carbon nanotube reinforced polymer composites in various engineering fields has led to the realization of many researches on the vibration problems in the finite deflections. The vast majority of these publications are dedicated to the solution of free vibration problems the finite deflections [33–52]. Among these studies, attention is drawn to the extensive studies by Shen et. al. [33,34,37,43,44] and Duc and co-authors [35,37–39,45,46] on the linear and nonlinear free vibrations and post-buckling problems of structural systems reinforced by carbon nanotubes in various media.

Previous research on the mechanics of CNT-based structural systems can be used as useful information for further development and validation of structural systems reinforced by CNTs. The mathematical complexity and lack of technology faced by dynamic shell analysis until recent years have made it difficult to achieve numerous new results for design applications. The literature review reveals that the nonlinear forced vibrations of CNT-patterned structural systems have not been adequately investigated. In this article, the authors try to solve this issue. Hamilton principle and von Karman-type nonlinear theory are used to obtain the theoretical model of structural systems reinforced by CNTs. The main goal of this study is to solve the problem of forced vibrations of structural systems reinforced by CNTs in the finite deflection using Galerkin and multi-scales methods, as well as to create a dependence of the nonlinear frequency on the amplitude of forced vibrations in the presence of viscous damping. This study is one of the first to use these approaches to investigate the nonlinear forced vibration behavior of structural systems reinforced by CNTs in the presence of viscous damping at primary resonance. Since double-curved shells can be transformed into other structural systems such as spherical shell, hyperbolic-paraboloid shell, rectangular plate and cylindrical panel in special cases, the expressions for nonlinear frequencies can also be used for them. The secondary goal is to obtain an analytical ratio of the nonlinear frequency of the forced vibration to the linear frequency, although perhaps not secondary to those interested in using the results. Finally, a systematic study is aimed at controlling the influence of nonlinearity and types of distribution of CNTs on the dependence of frequency on the amplitude of nonlinear forced vibrations and their quantitative and qualitative change in the presence of external excitation and viscous damping.

2. Formulation of the problem

The double-curved shell with the thickness h, the length a, the width b, and the mean radii of curvature r_1 and r_2, respectively, is subjected to external excitation loading, which depends on the time is shown in Fig. 1. The double-curved shells are transformed into spherical shells $r_1 = r_2$ plates and panels in special cases. For example, the double-curved shell transforms into a spherical shell, when $r_1 = r_2$, a hyperbolic paraboloid shell, when $r_1 = -r_2$, a panel, when $r_1 \to \infty$, and a rectangular plate, when $r_1 = r_2 \to \infty$. The orthogonal coordinate system (x, y, z) is located on the mid-surface of the double-curved shell, and the x, y and z coordinates are oriented in the direction of length, width, and thickness, respectively. The displacement components of the double-curved shell in the

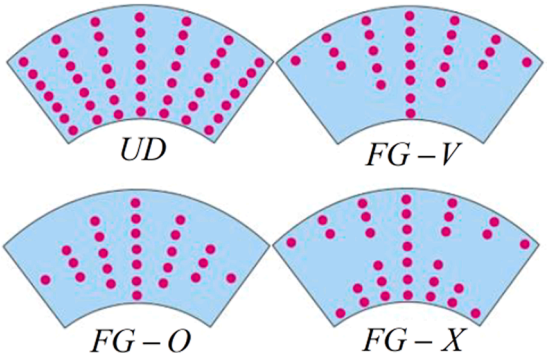

Fig. 2. Distribution of the volume fraction of CNTs over the matrix thickness.

x, y and z directions are denoted as u, v and w, respectively.

2.1. Material properties

According to the rule of mixture model, the effective material properties of the nanocomposites can be approximated as [32]:

$$E_{11}^{\bar{z}} = \eta_1 V_{cnt}^{\bar{z}} E_{11}^{cnt} + V_m E_m,\ E_{22}^{\bar{z}} = \frac{\eta_2 E_m E_{22}^{cnt}}{E_{22}^{cnt} V_m + E_m V_{cnt}^{\bar{z}}},\ G_{12}^{\bar{z}} = \frac{\eta_3 G_m G_{12}^{cnt}}{G_{12}^{cnt} V_m + G_m V_{cnt}^{\bar{z}}}$$
$$\nu_{12} = V_{cnt}^{*} \nu_{12}^{cnt} + V_m \nu_m,\ \rho_1 = V_{cnt}^{\bar{z}} \rho^{cnt} + V_m \rho_m,\ \bar{z} = z/h \tag{1}$$

where E_m, G_m, ρ_m, ν_m are, respectively, the Young's modulus, shear modulus, density and Poisson's ratio for the matrix, and E_{ij}^{cnt}, G_{ij}^{cnt}, ρ^{cnt}, $\nu_{12}^{cnt}(i,j=1,2)$ are their corresponding properties for the reinforcing CNT phase, $\eta_i(i=1,2,3)$ are the efficiency parameters, that define scale-dependent material properties. Here $V_{cnt}^{\bar{z}}$ and V_m are the volume fraction of CNTs and matrix that obey the rule of $V_{cnt}^{\bar{z}} + V_m = 1$. Here V_{cnt}^{*} is the total volume fraction of CNTs associated with the mass fraction (M^{cnt}) of CNTs and the densities of the constituents, which can be represented as:

$$V_{cnt}^{*} = \frac{M^{cnt}}{M^{cnt} + (\rho^{cnt}/\rho_m)(1 - M^{cnt})} \tag{2}$$

The distribution of the volume fraction of CNTs over the polymer matrix thickness as uniform (UD) and three types of linear functions is shown in Fig. 2 [32]:

$$V_{cnt}^{\bar{z}} = \begin{cases} UD & for\ \ V_{cnt}^{*} \\ FG-V & for\ \ 2(0.5-\bar{z})V_{cnt}^{*} \\ FG-O & for\ \ 2(0.5+\bar{z})V_{cnt}^{*} \\ FG-X & for\ \ 4|\bar{z}|\,V_{cnt}^{*} \end{cases} \tag{3}$$

2.2. Constitutive relations and basic equations

The constitutive relations of structural systems reinforced by CNTs in the scope of the classical shell theory can be expressed as follows [33,51]:

$$\begin{bmatrix} \sigma_{11} \\ \sigma_{22} \\ \sigma_{12} \end{bmatrix} = \begin{bmatrix} A_{11}^{\bar{z}} & A_{12}^{\bar{z}} & 0 \\ A_{21}^{\bar{z}} & A_{22}^{\bar{z}} & 0 \\ 0 & 0 & A_{66}^{\bar{z}} \end{bmatrix} \begin{bmatrix} \varepsilon_{11} \\ \varepsilon_{22} \\ \gamma_{12} \end{bmatrix} \tag{4}$$

where σ_{ij} and $\varepsilon_{ij}, \gamma_{ij}(i,j=1,2)$ are the stress and strains of structural systems reinforced by CNTs, respectively and the parameters $A_{ij}^{\bar{z}}$ are defined as

$$A_{11}^{\bar{z}} = \frac{E_{11}^{\bar{z}}}{1-\nu_{12}\nu_{21}},\ A_{22}^{\bar{z}} = \frac{E_{22}^{\bar{z}}}{1-\nu_{12}\nu_{21}},\ A_{12}^{\bar{z}} = \frac{\nu_{21}E_{11}^{\bar{z}}}{1-\nu_{12}\nu_{21}} = \frac{\nu_{12}E_{22}^{\bar{z}}}{1-\nu_{12}\nu_{21}} = A_{21}^{\bar{z}},\ A_{66}^{\bar{z}} = G_{12}^{\bar{z}} \tag{5}$$

The stress resultants and couples for structural systems reinforced by CNTs are defined by [52,53]:

$$(T_{ij}, m_{ij}) = \int_{-h/2}^{h/2} (\sigma_{ij}, z\sigma_{ij}) \mathrm{d}z, \quad (i,j = 1,2) \tag{6}$$

The relations between force components and Airy stress function ϕ are defined by:

$$(T_{11}, T_{22}, T_{12}) = h(\phi_{,yy}, \ \phi_{,xx}, \ -\phi_{,xy}) \tag{7}$$

In the presence of linear viscous damping, the nonlinear dynamic stability and compatibility equations of structural systems reinforced by CNTs are derived using the Hamilton principle, as follows [52,53]:

$$m_{11,xx} + 2m_{11,xy} + m_{22,yy} + T_{11}/r_1 + T_{22}/r_2 + T_{11}w_{,xx} + 2T_{12}w_{,xy} + T_{22}w_{,yy} + p(t) = \overline{\rho}\ddot{w} + 2\xi\overline{\rho}\dot{w} \tag{8}$$

$$e_{11,yy} + e_{22,xx} - \gamma_{0,xy} = w_{,xy}^2 - w_{,xx}w_{,yy} - w_{,xx}/r_2 - w_{,yy}/r_1 \tag{9}$$

where $(,)$ and $(\cdot)$ denote the partial differentiations with respect to coordinates and time, respectively, t is a time, ξ is the viscous damping coefficient, $p(t)$ is a periodically changing external excitation, its concrete expression is explained in the next step, $\overline{\rho} = \int_{-h/2}^{h/2} V_{cnt}^{\overline{z}} \rho^{cnt} dz + V_m \rho_m h$, and e_{11}, e_{22}, γ are strains on the mid-surface of structural systems reinforced by CNTs and include the following nonlinear terms [52]:

$$\begin{bmatrix} e_{11} \\ e_{22} \\ \gamma_0 \end{bmatrix} = \begin{bmatrix} \mathrm{u}_{,\mathrm{x}} - \mathrm{w}/\mathrm{r}_1 + 0.5\mathrm{w}_{,\mathrm{x}}^2 \\ \mathrm{u}_{,\mathrm{y}} - \mathrm{w}/\mathrm{r}_2 + 0.5\mathrm{w}_{,\mathrm{y}}^2 \\ \mathrm{v}_{,\mathrm{x}} + \mathrm{u}_{,\mathrm{y}} + \mathrm{w}_{,\mathrm{x}}\mathrm{w}_{,\mathrm{y}} \end{bmatrix} \tag{10}$$

By using relations (4) and (6)-(9), the nonlinear forced vibration equations of double-curved shells reinforced by CNTs in the presence of linear viscous damping may be written as,

$$\begin{aligned} &c_{12}h\phi_{,xxxx} + (c_{11} - 2c_{31} + c_{22})h\phi_{,xxyy} + c_{21}h\phi_{,yyyy} - c_{13}w_{,xxxx} - (c_{14} + 2c_{32} + c_{23})w_{,xxyy} - c_{24}w_{,yyyy} \\ &+h\phi_{,xx}/r_2 + h\phi_{,yy}/r_1 + h\phi_{,yy}w_{,xx} - 2h\phi_{,xy}w_{,xy} + h\phi_{,xx}w_{,yy} + p(t) = \overline{\rho}\ddot{w} + 2\xi\overline{\rho}\dot{w} \end{aligned} \tag{11}$$

$$\begin{aligned} &hb_{11}\phi_{,yyyy} + h(b_{12} + b_{21} + b_{31})\phi_{,xxyy} + hb_{22}\phi_{,xxxx} - b_{23}w_{,xxxx} - (b_{24} + b_{13} - b_{32})w_{,xxyy} \\ &-b_{14}w_{,yyyy} + \left(w_{,xx}/r_2 + w_{,yy}/r_1\right) - w_{,xy}^2 + w_{,xx}w_{,yy} = 0 \end{aligned} \tag{12}$$

where c_{ij} and $b_{ij} (i,j = 1,2,...,4)$ are defined as:

$$\begin{aligned} &c_{11} = \mathrm{u}_{11}^1\mathrm{b}_{11} + \mathrm{u}_{12}^1\mathrm{b}_{21}, \ c_{12} = \mathrm{u}_{11}^1\mathrm{b}_{12} + \mathrm{u}_{12}^1\mathrm{b}_{11}, \ c_{13} = \mathrm{u}_{11}^1\mathrm{b}_{13} + \mathrm{u}_{12}^1\mathrm{b}_{23} + \mathrm{u}_{11}^2, \ c_{14} = \mathrm{u}_{11}^1\mathrm{b}_{14} + \mathrm{u}_{12}^1\mathrm{b}_{24} + \mathrm{u}_{12}^2, \\ &c_{21} = \mathrm{u}_{21}^1\mathrm{b}_{11} + \mathrm{u}_{22}^1\mathrm{b}_{21}, \ c_{22} = \mathrm{u}_{21}^1\mathrm{b}_{12} + \mathrm{u}_{22}^1\mathrm{b}_{22}, \ c_{23} = \mathrm{u}_{21}^1\mathrm{b}_{13} + \mathrm{u}_{22}^1\mathrm{b}_{23} + \mathrm{u}_{21}^2, \ c_{24} = \mathrm{u}_{21}^1\mathrm{b}_{14} + \mathrm{u}_{22}^1\mathrm{b}_{24} + \mathrm{u}_{22}^2, \\ &c_{31} = \mathrm{u}_{66}^1\mathrm{b}_{35}, \ c_{32} = \mathrm{u}_{66}^1\mathrm{b}_{32} + 2\mathrm{u}_{66}^2, \ \mathrm{b}_{11} = \frac{\mathrm{u}_{22}^0}{\Lambda}, \ \mathrm{b}_{12} = -\frac{\mathrm{u}_{12}^0}{\Lambda}, \ \mathrm{b}_{13} = \frac{\mathrm{u}_{12}^0\mathrm{u}_{21}^1 - \mathrm{u}_{11}^1\mathrm{u}_{22}^0}{\Lambda}, \\ &b_{14} = \frac{u_{12}^0u_{22}^1 - u_{12}^1u_{22}^0}{\Lambda}, \ b_{21} = -\frac{u_{21}^0}{\Lambda}, \ b_{22} = \frac{u_{11}^0}{\Lambda}, \ b_{23} = \frac{u_{11}^1u_{21}^0 - u_{21}^1u_{11}^0}{\Lambda}, \ b_{24} = \frac{u_{12}^1u_{21}^0 - u_{22}^1u_{11}^0}{\Lambda}, \\ &b_{31} = \frac{1}{u_{66}^0}, \ b_{32} = -\frac{2u_{66}^1}{u_{66}^0}, \ \Lambda = u_{11}^0u_{22}^0 - u_{12}^0u_{21}^0, \ u_{11}^k = \int_{-h/2}^{h/2} A_{11}^{\overline{z}} z^k \mathrm{d}z, \ \mathrm{u}_{12}^{\mathrm{k}} = \int_{-\mathrm{h}/2}^{\mathrm{h}/2} \nu_{21}\mathrm{A}_{11}^{\overline{\mathrm{z}}}\mathrm{z}^{\mathrm{k}}\mathrm{d}z, \\ &u_{21}^k = \int_{-h/2}^{h/2} \nu_{12}A_{22}^{\overline{z}} z^k \mathrm{d}z, \ \mathrm{u}_{22}^{\mathrm{k}} = \int_{-\mathrm{h}/2}^{\mathrm{h}/2} \mathrm{A}_{22}^{\overline{\mathrm{z}}}\mathrm{z}^{\mathrm{k}}\mathrm{d}z, \ \mathrm{u}_{66}^{\mathrm{k}} = \int_{-\mathrm{h}/2}^{\mathrm{h}/2} \mathrm{A}_{66}^{\overline{\mathrm{z}}}\mathrm{z}^{\mathrm{k}}\mathrm{d}z, \ \mathrm{k} = 0,1,2. \end{aligned} \tag{13}$$

3. Methods of solution

Since the double-curved shell reinforced by CNTs obeys simply-supported boundary conditions, its mathematical model is expressed as follows [52–54]:

$$\begin{aligned} &w = 0, \ \mathrm{w}_{,\mathrm{yy}} = 0, \ \text{as } \mathrm{x} = 0 \text{ and } \mathrm{x} = \mathrm{a} \\ &w = 0, \ \mathrm{w}_{,\mathrm{xx}} = 0 \text{ as } \mathrm{y} = 0 \text{ and } \mathrm{y} = \mathrm{b} \end{aligned} \tag{14}$$

The solution of basic equations will be sought in the form, which $w(x,y,t)$ satisfies the simply-supported boundary conditions [54]:

$$\begin{aligned} w(x,y,t) &= \sum\nolimits_{\mathrm{m,n}}^{\infty} \overline{\mathrm{w}}_{\mathrm{mn}}(\mathrm{t}) \sin(\mathrm{m}_1\mathrm{x}) \sin(\mathrm{m}_2\mathrm{y}) \\ \phi(x,y,t) &= \sum\nolimits_{m=1}^{\infty} \overline{B}_{mn}(t)cos(2m_1x) + \sum\nolimits_{n=1}^{\infty} \overline{C}_{mn}(t)cos(2m_2y) + \sum\nolimits_{m=1}^{\infty}\sum\nolimits_{n=1}^{\infty} \overline{D}_{mn}(t)sin(m_1x)sin(i_2y) \end{aligned} \tag{15}$$

were $m_1 = \frac{m\pi}{a}$, and $m_2 = \frac{n\pi}{b}$ in which (m,n) denote vibration modes, $\overline{w}_{mn}(\mathrm{t})$, $\overline{B}_{mn}(t)$, $\overline{C}_{mn}(t)$ and $\overline{D}_{mn}(t)$ are time dependent unknown

functions, in which $\overline{B}_{mn}(t)$, $\overline{C}_{mn}(t)$ and $\overline{D}_{mn}(t)$ are found from the particular solutions of the inhomogeneous differential Eq. (8). Also, $\overline{B}_{mn}(t)$ and $\overline{C}_{mn}(t)$ are quadratic functions, and $\overline{D}_{mn}(t)$ is the first order function of $\overline{w}_{mn}(t)$.

The functions $w(x,y,t)$ and $\phi(x,y,t)$, which are sought in the above form, satisfy the deformation compatibility Eq. (9). The examples of determining these functions under various boundary conditions are presented in Pekerman and Galimov [54]. Based on the studies [52,54], the following expression can be used for $w(x,y,t)$, since the fundamental mode is more important in the primary resonance:

$$w = \overline{w}(t)\sin(m_1 x)\sin(m_2 y) \tag{16}$$

Letting (16) into Eq. (12), the Airy stress function is found from the particular solutions of the inhomogeneous differential equation as follows:

$$\phi = p_1\overline{w}^2(t)cos(2m_1x) + p_2\overline{w}^2(t)cos(2m_2y) + p_3\overline{w}(t)sin(m_1x)sin(m_2y) \tag{17}$$

where

$$p_1 = \frac{m_2^2}{32m_1^2b_{22}h},\ p_2 = \frac{m_1^2}{32m_2^2b_{11}h},\ p_3 = \frac{b_{23}m_1^4 + (b_{24}+b_{13}-b_{32})m_1^2m_2^2 + b_{14}m_2^4 + m_1^2/r_2 + m_2^2/r_1}{b_{11}hm_2^4 + (b_{12}+b_{21}+b_{31})hm_1^2m_2^2 + b_{22}hm_1^4} \tag{18}$$

By applying Galerkin method to the Eq. (11) in the ranges of $0\leqslant x\leqslant a$ and $0\leqslant y\leqslant b$, and introducing (16) and (17) into the nonlinear motion equation (11), we obtain the following ordinary nonlinear differential equation:

$$\ddot{\overline{w}} + 2\xi\dot{\overline{w}} + \Omega_0^2\overline{w} + \delta_{12}\overline{w}^2 + \delta_{13}\overline{w}^3 - \delta_{14}p(t) = 0 \tag{19}$$

where Ω_0 is the natural frequency of double-curved structural systems reinforced by CNTs and expressed as:

$$\Omega_0 = \sqrt{\delta_{11}} \tag{20}$$

in which

$$\begin{aligned}
\delta_{11} &= \overline{\rho}^{-1}\left\{\left[m_1^2/r_2 + m_2^2/r_1 - c_{12}m_1^4 - (c_{11} - 2c_{31} + c_{22})m_1^2m_2^2 - c_{21}m_2^4\right]hp_3\right.\\
&\quad \left. + c_{13}m_1^4 + (c_{14} + 2c_{32} + c_{24})m_1^2m_2^2 + c_{24}m_2^4\right\},\\
\delta_{12} &= 64h\overline{\rho}^{-1}a^{-1}b^{-1}[1-(-1)^m-(-1)^n+(-1)^{m+n}]\times\\
&\quad \times\left(c_{12}m_1^3p_1/m_2 + c_{21}m_2^3p_2/m_1 - 0.125m_1m_2p_3 - 0.25p_1m_1/r_2m_2 - 0.25p_2m_2/r_1m_1\right)/3\\
\delta_{13} &= 2hm_1^2m_2^2(p_1+p_2)\overline{\rho}^{-1},\quad \delta_{14} = 4\overline{\rho}^{-1}m^{-1}n^{-1}\pi^{-2}[1-(-1)^m-(-1)^n+(-1)^{m+n}]
\end{aligned} \tag{21}$$

The initial conditions are given as: $\overline{w}|_{t=0} = \overline{w}_{max}$, $\left.\frac{d\overline{w}}{dt}\right|_{t=0} = 0$.

Suppose that the external excitation, $p(t)$, changes harmonically [55]:

$$p(t) = P_0cos(\vartheta t) \tag{22}$$

where ϑ and P_0 are the frequency and amplitude of the time-depending harmonic excitation, respectively.

Introducing (22) into the Eq. (19), the differential equation of the nonlinear forced vibration for structural systems reinforced by CNTs in the presence of linear viscous damping is obtained as follows:

$$\ddot{\overline{w}} + 2\xi\dot{\overline{w}} + \Omega_0^2\overline{w} + \delta_{12}\overline{w}^2 + \delta_{13}\overline{w}^3 - \delta_{14}P_0cos(\vartheta t) = 0 \tag{23}$$

For the occurrence of primary resonance, must be provided $\vartheta \approx \Omega_0$, and damping, nonlinearity and excitation must be included at the same time in the disturbance circuit to analyze this case. The nonlinearity produces a term proportional to $cos(\Omega_0 t)$ for $O(\varepsilon^3)$. Here ε is a perturbation small parameter. We need order $2\xi\dot{\overline{w}}(t)$, as the $2\varepsilon^2\overline{\xi}\dot{\overline{w}}(t)$, and $\delta_{14}P_0cos(\vartheta t)$, as the $\varepsilon^2\overline{\delta}_{14}cos(\vartheta t)$, so that we can form the basic equation as follows:

$$\ddot{\overline{w}}(t) + \Omega_0^2\overline{w}(t) = -2\varepsilon^2\overline{\xi}\dot{\overline{w}}(t) - \varepsilon\overline{\delta}_{12}\overline{w}^2(t) - \varepsilon^2\overline{\delta}_{13}\overline{w}^3(t) + \varepsilon^2\overline{\delta}_{14}cos(\vartheta t) \tag{24}$$

where the following definitions apply:

$$\overline{\xi} = \frac{\xi}{\varepsilon^2},\ \overline{\delta}_{12} = \frac{\delta_{12}}{\varepsilon},\ \overline{\delta}_{13} = \frac{\delta_{13}}{\varepsilon^2},\ \overline{\delta}_{14} = \frac{\delta_{14}P_0}{\varepsilon^2} \tag{25}$$

An approximate solution to the problem can be obtained by a series of perturbation techniques. Since the multi-scale method is used here, the solution is expressed in different time scales as follows [55]:

$$\overline{w}(t,\varepsilon) = \overline{w}_0(\tau_0,\tau_1,\tau_2) + \varepsilon\overline{w}_1(\tau_0,\tau_1,\tau_2) + \varepsilon^2\overline{w}_2(\tau_0,\tau_1,\tau_2) + \ldots \tag{26}$$

where $\tau_0 = t$, $\tau_1 = \varepsilon t$ and $\tau_2 = \varepsilon^2 t$. We also express the excitation in terms of τ_0 and τ_2 as $\overline{\delta}_{14}cos(\Omega_0\tau_0 + \sigma\tau_2)$. Since the excitation is O

(ε^2), ∂-Ω_0 is assumed to be $O(\varepsilon^2)$ for consistency. Hence, we put

$$\partial = \Omega_0 + \varepsilon^2\sigma \tag{27}$$

Substituting expressions (26) and (27) into Eq. (24) and equating the coefficients of ε^0, ε and ε^2 on the both sides, we obtain,

$$D_0^2\overline{w}_0 + \Omega_0^2\overline{w}_0 = 0 \tag{28}$$

$$D_0^2\overline{w}_1 + \Omega_0^2\overline{w}_1 = -2D_0D_1\overline{w}_0 - \overline{\delta}_{12}\overline{w}_0^2 \tag{29}$$

$$\begin{aligned} D_0^2\overline{w}_2 + \Omega_0^2\overline{w}_2 = {} & -2D_0D_1\overline{w}_1 - 2D_0D_2\overline{w}_0 - D_1^2\overline{w}_0 - 2\overline{\xi}D_0\overline{w}_0 \\ & -2\overline{\delta}_{12}\overline{w}_0\overline{w}_1 - \overline{\delta}_{13}\overline{w}_0^3 + \overline{\delta}_{14}cos(\Omega_0\tau_0 + \sigma\tau_2) \end{aligned} \tag{30}$$

where $D_n = \frac{\partial}{\partial\tau_n}(n = 0,1,2)$. The general solution of the Eq. (28) is obtained as follows:

$$\overline{w}_0 = A(\tau_1,\tau_2)e^{i\Omega_0\tau_0} + \overline{A}(\tau_1,\tau_2)e^{-i\Omega_0\tau_0} \tag{31}$$

where $A(\tau_1,\tau_2)$ and $\overline{A}(\tau_1,\tau_2)$ are unknown functions. Substituting expression (31) into Eq. (29) yields,

$$D_0^2\overline{w}_1 + \Omega_0^2\overline{w}_1 = -2i\Omega_0D_1Ae^{i\Omega_0\tau_0} - \overline{\delta}_{12}\left[A^2e^{2i\Omega_0\tau_0} + A\overline{A}\right] + C_1 \tag{32}$$

Eliminating the terms in Eq. (32) that procedure secular terms in $\overline{w}_1$ gives $D_1A = 0$, or $A = A(\tau_2)$. Therefore, the solution of Eq. (32) is as follows:

$$\overline{w}_1 = \frac{\overline{\delta}_{12}}{\Omega_0^2}\left(-2A\overline{A} + \frac{1}{3}A^2e^{2i\Omega_0\tau_0} + \frac{1}{3}A^2e^{-2i\Omega_0\tau_0}\right) \tag{33}$$

Substituting expressions (31) and (33) into Eq. (30), yields

$$D_0^2\overline{w}_2 + \Omega_0^2\overline{w}_2 = -\left[2i\Omega_0(A' + \overline{\xi}A) + \left(3\overline{\delta}_{13} - \frac{10\overline{\delta}_{12}^2}{3\Omega_0^2}\right)A^2\overline{A} - \frac{1}{2}\overline{\delta}_{14}e^{i\sigma\tau_2}\right]e^{i\Omega_0\tau_0} + C_1 + NST \tag{34}$$

where $A' = \frac{\partial A}{\partial\tau_2}$, C_1 is stands for the complex conjugate of the preceding terms, the prime denotes the derivatives with respect to τ_2 and NST stands for terms proportional to $e^{\pm 3i\Omega_0\tau_0}$ [55]. Secular terms will be eliminated form (34) if

$$2i\Omega_0(A' + \overline{\xi}A) + \left(3\overline{\delta}_{13} - \frac{10\overline{\delta}_{12}^2}{3\Omega_0^2}\right)A^2\overline{A} - \frac{1}{2}\overline{\delta}_{14}e^{i\sigma\tau_2} = 0 \tag{35}$$

To solve the Eq. (35), we write parameter A in the polar form as,

$$A = \frac{1}{2}\alpha e^{i\beta} \tag{36}$$

where α and β are the amplitude and phase. Then substituting expression (36) into Eq. (35), we separate the result into its real and imaginary parts and obtain

$$\alpha' = -\overline{\xi}\alpha + \frac{\overline{\delta}_{14}}{2\Omega_0}sin\gamma \tag{37}$$

$$\alpha\beta' = \frac{9\overline{\delta}_{13}\Omega_0^2 - 10\overline{\delta}_{12}^2}{24\Omega_0^3}\alpha^3 - \frac{\overline{\delta}_{14}}{2\Omega_0}cos\gamma \tag{38}$$

where $\alpha' = \frac{\partial\alpha}{\partial\tau_2}$, $\beta' = \frac{\partial\beta}{\partial\tau_2}$ and γ is the new phase angle and defined as:

$$\gamma = \sigma\tau_2 - \beta \tag{39}$$

Eliminating β from Eqs. (38) and (39), yields

$$\alpha\gamma' = \alpha\sigma - \frac{9\overline{\delta}_{13}\Omega_0^2 - 10\overline{\delta}_{12}^2}{24\Omega_0^3}\alpha^3 + \frac{\overline{\delta}_{14}}{2\Omega_0}cos\gamma \tag{40}$$

Steady-state motions occur when $\gamma' = \alpha' = 0$, which corresponds to the singular points of Eqs. (37) and (38), that is they correspond to the solutions,

Table 1
The efficiency parameters and total volume fraction of CNTs.

V_{cnt}^{*}	η_1	η_2	η_3
0.12	0.137	1.022	0.715
0.17	0.142	1.626	1.138
0.28	0.141	1.585	1.109

Table 2
Comparison of the nonlinear to linear frequency ratio (Ω_{NL}/Ω_0) for homogeneous of orthotropic cylindrical shell with $(m = 1, n = 4)$

$\overline{\theta}$	Sheng and Wang [25]	Present
0.5	1.0017	1.00185
1.0	1.0066	1.00738
1.5	1.0149	1.01554
2.0	1.0265	1.02723
2.5	1.0414	1.04531

$$\begin{aligned} 0 &= -\overline{\xi}\alpha + \frac{\overline{\delta}_{14}}{2\Omega_0} sin\gamma \\ 0 &= \alpha\sigma - \frac{9\overline{\delta}_{13}\Omega_0^2 - 10\overline{\delta}_{12}^2}{24\Omega_0^3}\alpha^3 + \frac{\overline{\delta}_{14}}{2\Omega_0} cos\gamma \end{aligned} \tag{41}$$

The Eq. (41) is an implicit equation for the amplitude of the response α as a function of the detuning parameter σ (i.e., the frequency of the excitation) and the amplitude of the excitation $\overline{\delta}_{14}$; it is called the frequency–response equation. This solution method is called multi-scale method.

From Eq. (41), the second order approach of the frequency–response curve for the desired (m, n) mode for structural systems reinforced by CNTs is obtained as follows:

$$\sigma_{1,2} = \Gamma h^2\overline{\theta}^2 \pm \sqrt{\frac{\overline{\delta}_{14}^2}{4\Omega_0^2 h^2\overline{\theta}^2} - \overline{\xi}^2} \tag{42}$$

where the $\theta = \alpha/h$ is the dimensionless vibration amplitude, Γ defines the nonlinear vibration behavior of structural systems reinforced by CNTs and is found in the following expression:

$$\Gamma = \frac{1}{8\Omega_0}\left(3\overline{\delta}_{13} - \frac{10\overline{\delta}_{12}^2}{3\Omega_0^2}\right) \tag{43}$$

The dimensionless nonlinear forced vibration frequencies structural systems reinforced by CNTs for the primary resonance are expressed as:

$$\vartheta_{Forc}^{(i)} = \left(\Omega_0 + \varepsilon^2\sigma_i\right)h\sqrt{\rho_m/E_m} \ (i = 1, 2) \tag{44}$$

The nonlinear forced vibration frequency to the linear forced vibration frequency ratio of structural systems reinforced by CNTs is defined as

$$\vartheta_{Forc}^{(i)}/\Omega_0 = 1 + \varepsilon^2\sigma_i/\Omega_0 \ (i = 1, 2) \tag{45}$$

In the absence of external excitation, that is, when $P_0 = 0$ and damping is zero, that is, $\xi = 0$, the backbone curve of structural systems reinforced by CNTs is obtained.

The expressions (42), (44) and (45) for double-curved shells reinforced by CNTs also apply to other structural systems such as spherical shells, hyperbolic paraboloidal shells, cylindrical panels and plates reinforced by CNTs, as $r_1 = r_2$, $r_1 = -r_2$, $r_1 \to \infty$ and $r_1 = r_2 \to \infty$, respectively.

4. Numerical applications

4.1. Material properties of CNTs and matrix

In this subsection, the material point of view, polymethyl methacrylate (PMMA) is considered as a matrix with the properties: $E_m = 2.5$ GPa, $\nu_m = 0.34$, $\rho_m = 1150$ kg/m^3. In addition, SWCNTs as reinforcement with (10, 10) armchair structure with the material

Table 3
Comparison of non-dimensional natural frequency parameters for composite plates with different CNT patterns and modes

	Selim et al. [56]	Present study	Selim et al. [56]	Present study	Selim et al. [56]	Present study	Selim et al. [56]	Present study
Mode	UD		FG-V		FG-O		FG-X	
1	23.659	24.116	19.950	20.209	17.502	17.694	28.345	29.179
2	28.942	29.328	26.166	26.386	23.745	23.907	33.354	34.075
3	43.106	42.972	41.594	41.346	38.823	38.525	47.444	47.571

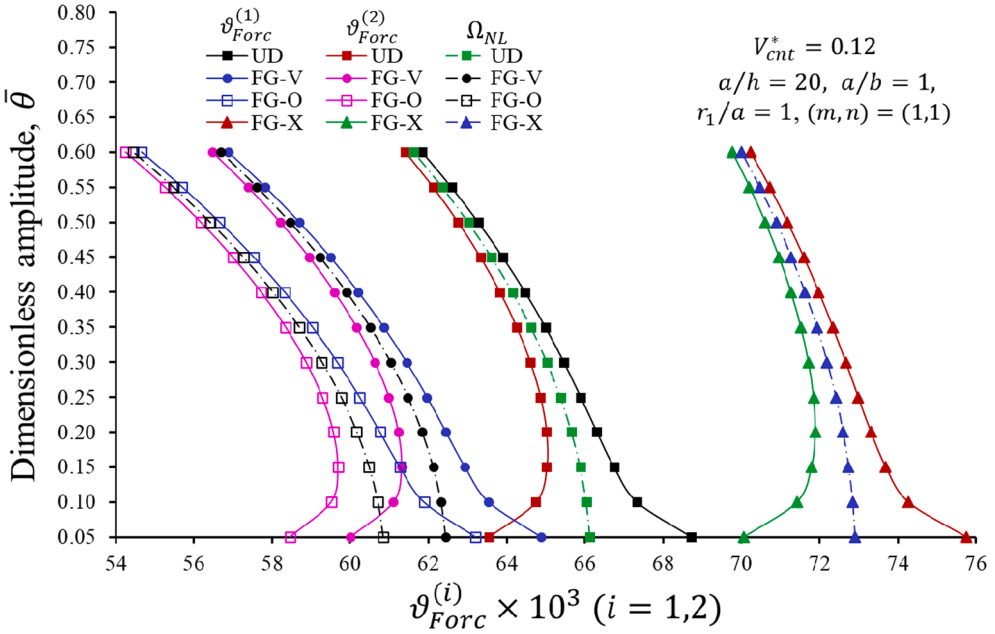

Fig. 3. Distribution of $\vartheta_{Forc}^{(1)}$, $\vartheta_{Forc}^{(2)}$ and backbone curve for UD and FG patterned structural systems according to the dimensionless amplitude $\bar{\theta}$.

properties: $\bar{r} = 9.26\,\text{nm}$, $\bar{a} = 0.68\,\text{nm}$, $\bar{h} = 0.067\,\text{nm}$, and $E_{11}^{cnt} = 5.6466\,\text{TPa}$, $E_{22}^{cnt} = 7.08\,\text{TPa}$, $G_{12}^{cnt} = 1.9445\,\text{TPa}$, $\nu_{12}^{cnt} = 0.175$, $\rho_{cnt} = 1400\,\text{kg/m}^3$ at room temperature (T = 300 K). The efficiency parameters and total volume fraction of CNTs are presented in Table 1 [32].

4.2. Examples for validation

In order to verify the present results, Ω_{NL}/Ω_0 for homogeneous orthotropic shells are compared with the results of Sheng and Wang [25] and given Table 2. The nonlinear free vibration frequency Ω_{NL} is defined as $\Omega_{NL} = \Omega_0 + \varepsilon^2\sigma_1$, in which the detuning parameter σ_1 is obtained by setting $\xi_1 = 0$ (without damping), $\bar{\delta}_{14} = 0$ (without excitation) $V_{cnt}^{\bar{z}} = 0$ in the Eq. (42). The orthotropic material properties and shell parameters are as follows: $b = 1.5748r_2$, $r_1 \to \infty$, $r_2 = 100h$, $E_{11}^{m} = 200\,\text{GPa}$, $E_{22}^{m} = G_{12}^{m} = 10\,\text{GPa}$, $\nu_{12} = 0.2$, $\rho_m = 7800\,\text{kg/m}^3$. It can be seen from Table 2 that the results are in agreement.

In a second example, our results are compared with the study in Ref. [56] which gives the dimensionless frequency parameter of linear free vibration of composite plates with different CNT patterns and for different modes. To transform double-curved shells into rectangular plates, $r_1 \to \infty$, $r_2 \to \infty$ is taken into account in the Eq. (20). For comparison, are used the data $V_{cnt}^{*} = 0.17$, $a/b = 1$, $b/h = 50$, which were taken from ref. [56]. The dimensionless frequency parameter is calculated using the formula $\Omega_{1s} = \Omega_0\left(b^2/h\right)\sqrt{\rho^m/E^m}$. Table 3 shows that the dimensionless frequency parameters for all modes and the patterns of CNTs are in good agreement.

4.3. Unique examples of nonlinear forced vibration

The specific analyzes on the dimensionless nonlinear forced vibration frequency (DNFVF) of structural systems reinforced by CNTs are made based on Eqs. (44) and (45). In the all calculations the following data are used: $\varepsilon = 0.01$, $a/h = 20$ and $(m,n) = (1,1)$. The linear viscous damping effect is taken into account in Fig. 10. The shell geometries and other data are presented in each figure or in the comments section. In all calculations, except Figs. 7, 8 and 10 use the following expression for the external excitation: $P_0 = A_{p_0}h^2\rho_m\Omega_0^2$

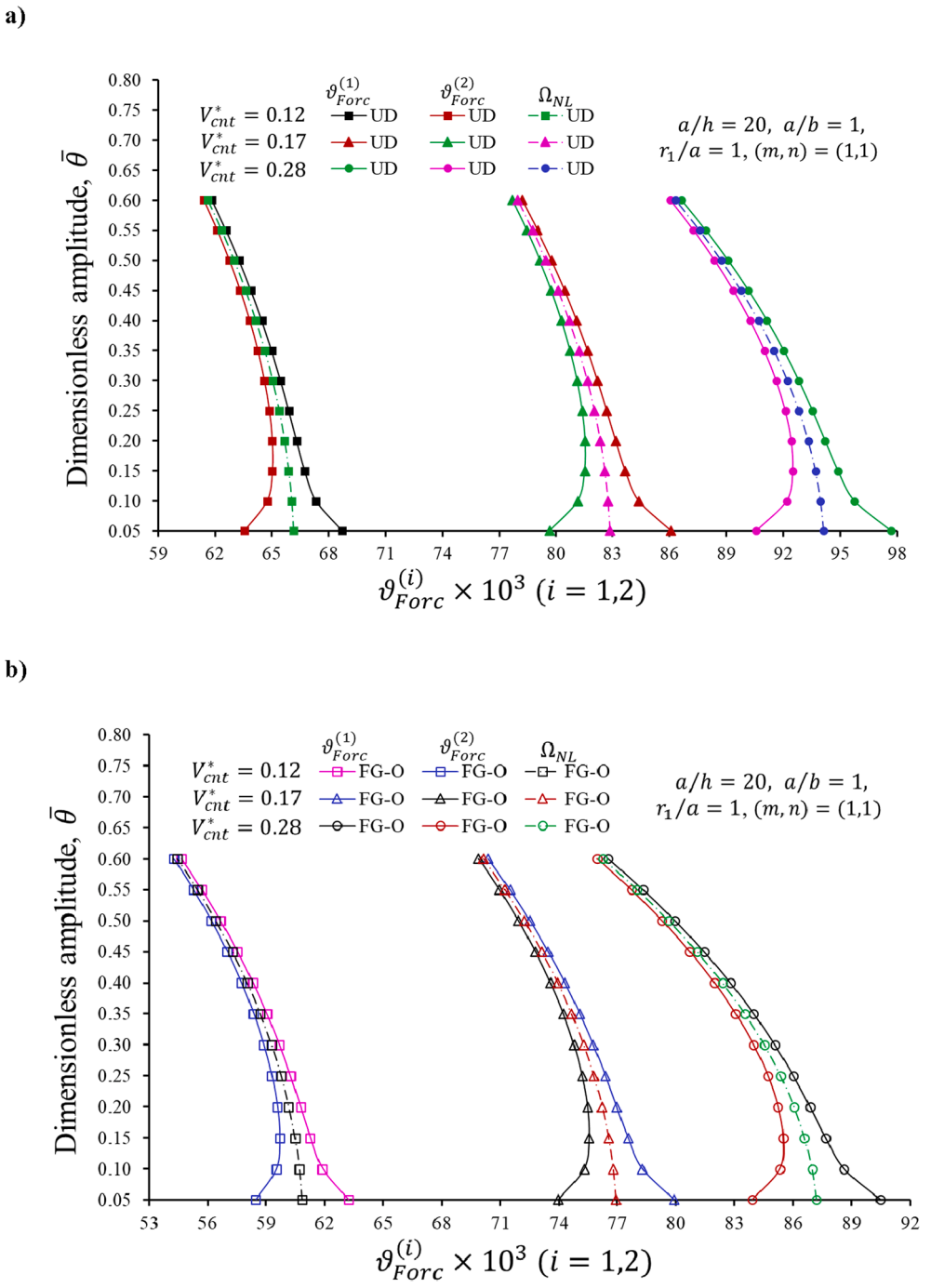

Fig. 4. Distribution of $\vartheta^{(1)}_{Forc}$, $\vartheta^{(2)}_{Forc}$ and backbone curve for a) UD and b) FG-O patterned structural systems according to $\bar{\theta}$ for different V^*_{cnt}.

in which the amplitude of the external excitation is considered as $A_{p_0} = 0.004$ [15,25].

The distributions of dimensionless nonlinear forced vibration frequencies $\vartheta^{(1)}_{Forc}$, $\vartheta^{(2)}_{Forc}$ and backbone curve of UD and structural systems reinforced by CNTs with UD, FG-V, FG-O and FG-X profiles according to the dimensionless amplitude, $\bar{\theta}$, for the data $V^*_{cnt} = 0.12,\ r_1/a = 1,\ a/h = 20,\ a/b = 1$ are plotted in Fig. 3. The backbone curve is between $\vartheta^{(1)}_{Forc}$ and $\vartheta^{(2)}_{Forc}$ curves in all calculations. Based on the data used, the magnitudes of the $\vartheta^{(1)}_{Forc}$ for spherical shells with all distribution types of CNTs throughout the thickness of the matrix, decreases due to the increase of the $\bar{\theta}$, while the magnitudes of $\vartheta^{(2)}_{Forc}$ increase first and then decrease after a certain value of the $\bar{\theta}$. Although the fastest decrease of $\vartheta^{(1)}_{Forc}$ and $\vartheta^{(2)}_{Forc}$ occur in the FG-O profile, the attenuation of these decrease is observed for FG-V, UD

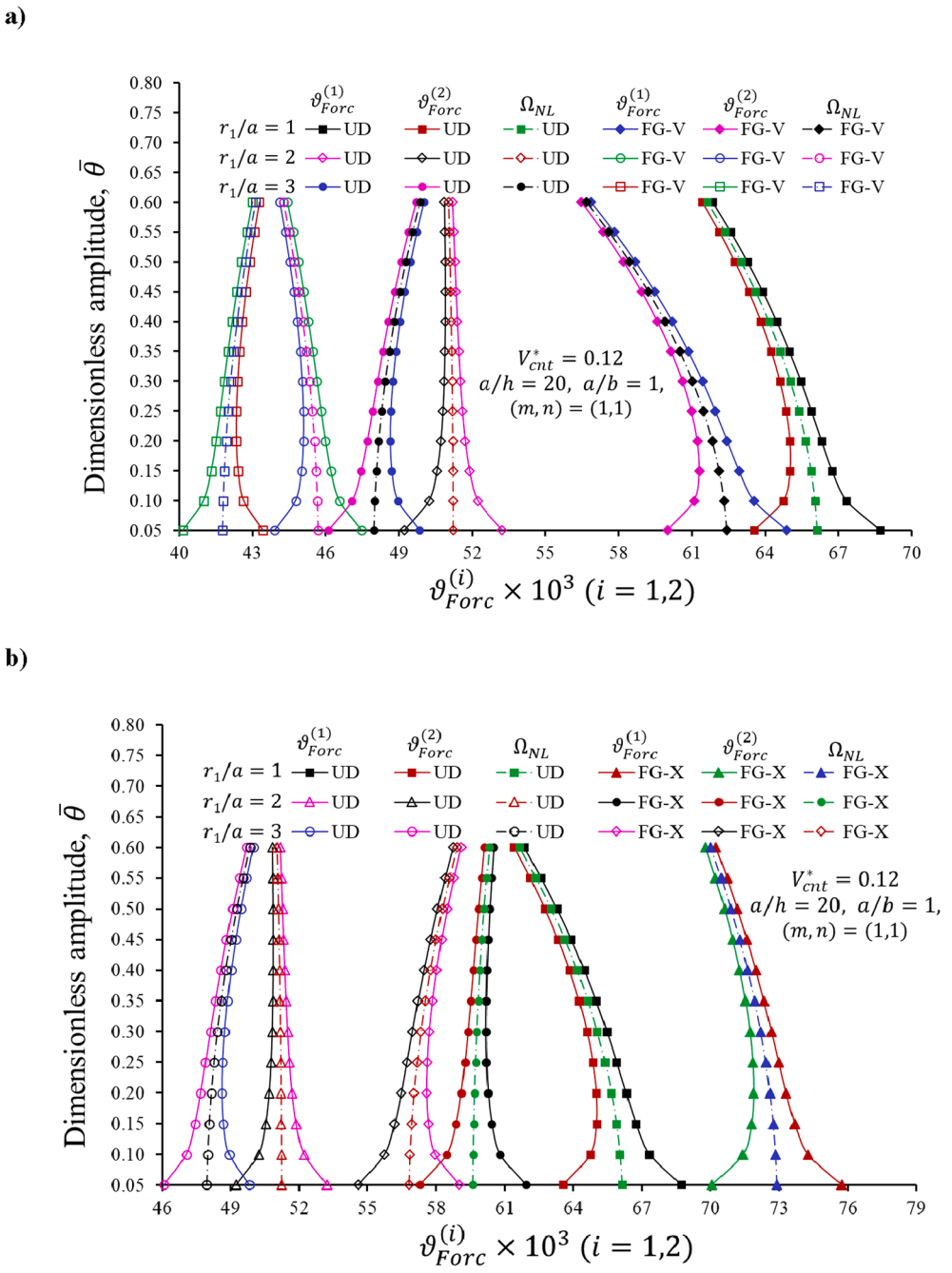

Fig. 5. Distribution of $\vartheta^{(1)}_{Forc}$, $\vartheta^{(2)}_{Forc}$ and backbone curve for a) UD and FG-V, and b) UD and FG-X patterned structural systems according to the $\overline{\theta}$ for different r_1/a.

and FG-X patterned structural systems, respectively. The influences of FG profiles on $\vartheta^{(1)}_{Forc}$ and $\vartheta^{(2)}_{Forc}$ increase due to the increase of the $\overline{\theta}$. The highest influence of FG profiles on $\vartheta^{(1)}_{Forc}$ and $\vartheta^{(2)}_{Forc}$ occurs in FG-X patterned structural systems. For instance, the influence of the FG-X profile on the DNFVF increases from (+10.24%) to (+13.6%), as $\overline{\theta}$ increases from 0.05 to 0.6.

In Fig. 4, the distribution of $\vartheta^{(1)}_{Forc}$, $\vartheta^{(2)}_{Forc}$ and backbone curve of UD and FG-O patterned structural systems according to $\overline{\theta}$ for different V^*_{cnt} and with following fixed data, $r_1/a = 1,\ a/h = 20,\ a/b = 1$ is illustrated. It is seen that the magnitudes of $\vartheta^{(1)}_{Forc}$ and backbone curve of UD and FG-O patterned structural systems decrease due to the increase of $\overline{\theta}$, whereas the values of $\vartheta^{(2)}_{Forc}$ increase up to $\overline{\theta} = 0.15$ and decrease in the next increment of $\overline{\theta}$. When the influences of $V^*_{cnt} = 0.12$, 0.17 and 0.28 on DNFVFs are compared among themselves, it

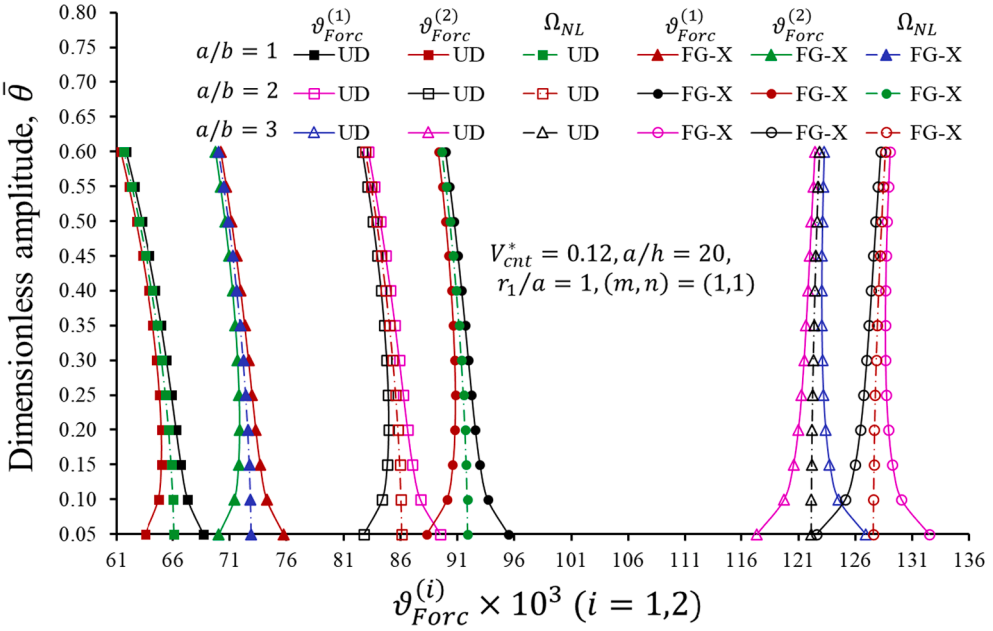

Fig. 6. Distribution of $\vartheta^{(1)}_{Forc}$, $\vartheta^{(2)}_{Forc}$ and backbone curve for UD and FG-X patterned structural systems according to $\overline{\theta}$ for different a/b.

has been determined that the greatest influence on $\vartheta^{(1)}_{Forc}$ and $\vartheta^{(2)}_{Forc}$ occurs at $V^*_{cnt} = 0.12$, while the least influence occurs at $V^*_{cnt} = 0.17$. Also, the influences of the FG-O profile on $\vartheta^{(1)}_{Forc}$ and $\vartheta^{(2)}_{Forc}$ increase depending on the increase of $\overline{\theta}$. For instance, the influences of the FG-O profile on DNFVFs for $V^*_{cnt} = 0.12,\ 0.17$ and 0.28 are (-8%), (-7.22%) and (-7.45%), respectively, at $\overline{\theta} = 0.1$, whereas those are (-10.5%), (-9.1%) and (-10.3%), respectively, at $\overline{\theta} = 0.5$.

The distributions of $\vartheta^{(1)}_{Forc}$, $\vartheta^{(2)}_{Forc}$ and backbone curve of UD, FG-V and FG-X- patterned structural systems according to $\overline{\theta}$, for fixed data $V^*_{cnt} = 0.12,\ a/h = 20,\ a/b = 1$ and with different r_1/a are illustrated in Fig. 5. For considered data, the magnitudes of $\vartheta^{(1)}_{Forc}$, $\vartheta^{(2)}_{Forc}$ and backbone curve for UD and structural systems reinforced by CNTs decrease, as the r_1/a ratio increases. The magnitudes of $\vartheta^{(1)}_{Forc}$ for FG-V and FG-X patterned structural systems continuously decrease due to the increase of $\overline{\theta}$, while the magnitudes of $\vartheta^{(2)}_{Forc}$ first increase and then decrease by taking the maximum value, at $r_1/a = 1$. The magnitudes of $\vartheta^{(1)}_{Forc}$ for FG-V patterned structural systems for $r_1/a = 2$ change similarly to those of $r_1/a = 1$. The magnitudes of $\vartheta^{(1)}_{Forc}$ for FG-V and FG-X patterned structural systems first decrease and then increase due to the increase of the $\overline{\theta}$, while the values of the $\vartheta^{(2)}_{Forc}$ first increase and then decrease after a certain value of $\overline{\theta}$ for $r_1/a = 3$. Furthermore, the values of the $\vartheta^{(1)}_{Forc}$ for FG-X profile $r_1/a = 2$ change similarly to the $r_1/a = 3$ ratio. Also, the influences of FG-O and FG-X type distributions on $\vartheta^{(1)}_{Forc}$ and $\vartheta^{(2)}_{Forc}$ significantly increases with the increasing of the r_1/a ratio. For instance; the influences of FG-O and FG-X type distributions on $\vartheta^{(1)}_{Forc}$ and $\vartheta^{(2)}_{Forc}$ are (-8.1%) and $(+10.3\%)$, respectively, as $\overline{\theta} = 0.1$, while those are (-11.64%) and $(+13.6\%)$, respectively, as $\overline{\theta} = 0.6$ for $r_1/a = 1$ and $V^*_{cnt} = 0.12$. The influences of FG-O and FG-X profiles on $\vartheta^{(1)}_{Forc}$ and $\vartheta^{(2)}_{Forc}$ are (-14.57%) and $(+18.42\%)$, respectively, as $\overline{\theta} = 0.1$, whereas those are (-15.23%) and $(+18.19\%)$, respectively, as $\overline{\theta} = 0.6$ with $r_1/a = 3$ and $V^*_{cnt} = 0.12$.

The distribution of $\vartheta^{(1)}_{Forc}$, $\vartheta^{(2)}_{Forc}$ and backbone curve of UD and FG-X profiles according to $\overline{\theta}$ for fixed data $V^*_{cnt} = 0.12,\ r_1/a = 1$ and with different a/b is plotted in Fig. 6. The magnitudes of $\vartheta^{(1)}_{Forc}$, $\vartheta^{(2)}_{Forc}$ and backbone curve for UD and FG-X profiles increase, as a/b increases. At $a/b = 1$ and 2; while the magnitudes of $\vartheta^{(1)}_{Forc}$ for UD and FG-X patterned structural systems decrease due to increase of $\overline{\theta}$, the magnitudes of $\vartheta^{(2)}_{Forc}$ first increase and then decrease after the certain value of $\overline{\theta}$. The magnitudes of $\vartheta^{(1)}_{Forc}$ and $\vartheta^{(2)}_{Forc}$ for UD and FG-X type shells are increase due to increase of $\overline{\theta}$ at $a/b = 3$. At $a/b = 2$ compared to $a/b = 1$, it is observed that the rate decreases of DNFVF for FG-X profile structural systems reduce due to increase of $\overline{\theta}$, whereas the magnitudes of DNFVFs increases, at $a/b = 3$. Additionally, the increase of a/b significantly reduces the influence of the FG-X profile on the magnitudes of DNFVFs. For instance; the influences of the FG-X profile on the magnitudes of DNFVFs are: $(+10.24\%)$, $(+6.72\%)$ and $(+4.44\%)$ for $a/b = 1, 2$ and 3, respectively, as $V^*_{cnt} = 0.12$ and $\overline{\theta} = 0.05$. Furthermore, the influence of FG-X profile on $\vartheta^{(1)}_{Forc}$ and $\vartheta^{(2)}_{Forc}$ increases, as $\overline{\theta}$ increases, but increase of a/b significantly weakens the influence of FG-X on $\vartheta^{(1)}_{Forc}$ and $\vartheta^{(2)}_{Forc}$.

The distribution of nonlinear forced vibration and backbone curves of UD, FG-O and FG-X- patterned structural systems according to $\overline{\theta}$, for fixed data $V^*_{cnt} = 0.17,\ r_1/a = 2,\ a/b = 1$ and with different external excitation P_0 is described in Fig. 7. The magnitudes of

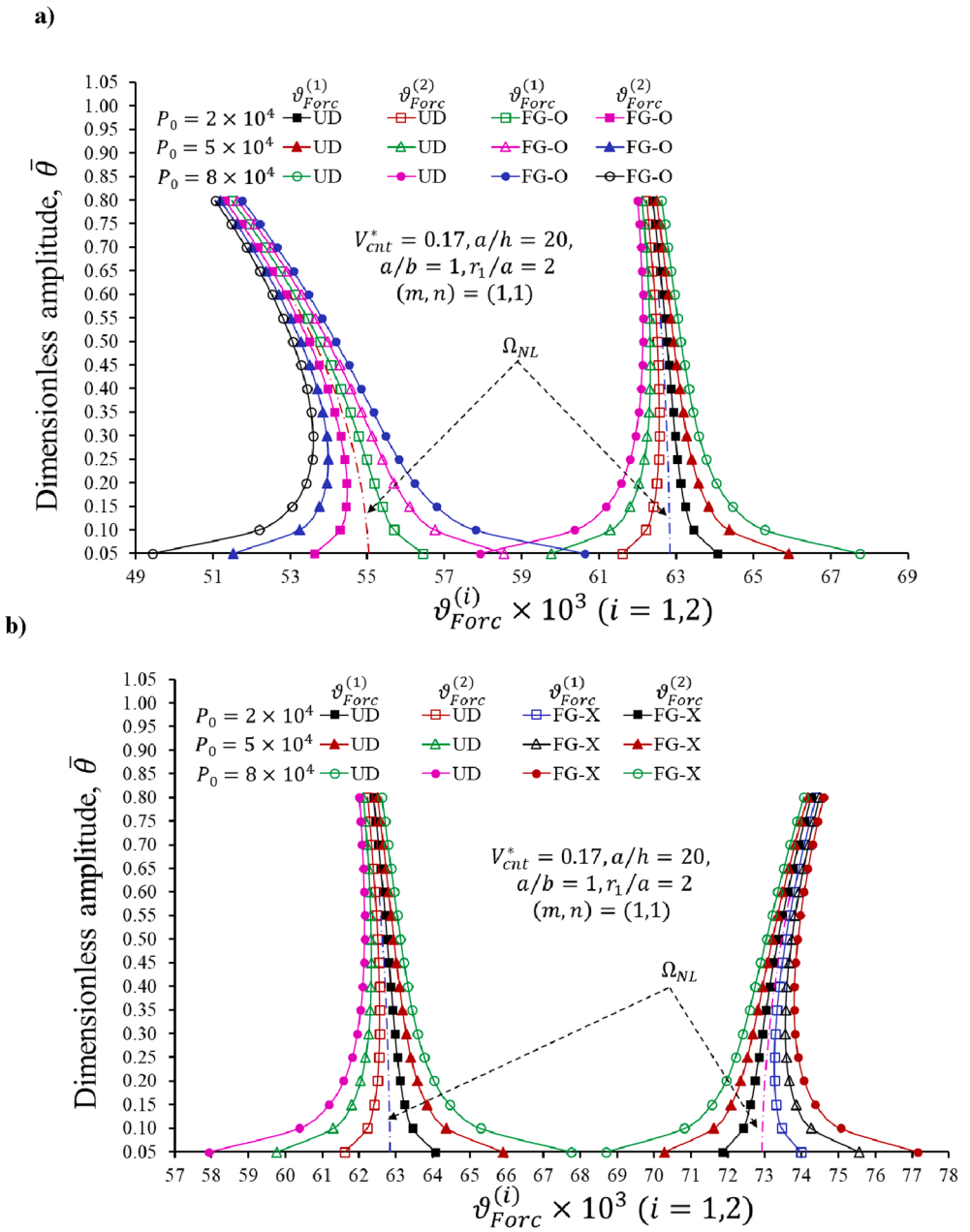

Fig. 7. Distribution of $\vartheta_{Forc}^{(1)}$, $\vartheta_{Forc}^{(2)}$ and backbone curve for a) UD and FG-O and b) UD and FG-X patterned structural systems according to $\bar{\theta}$ for different external excitation P_0.

$\vartheta_{Forc}^{(1)}$ for FG-O profile decreases, while $\vartheta_{Forc}^{(2)}$ increases first and then decreases due to the increase of $\bar{\theta}$, for all values of P_0. The magnitudes of $\vartheta_{Forc}^{(1)}$ for FG-X patterned structural systems first decreases and then increases due to increase of $\bar{\theta}$, while $\vartheta_{Forc}^{(1)}$ increases continuously for all values of P_0. While the increase of P_0 increases the values of $\vartheta_{Forc}^{(1)}$, the values of $\vartheta_{Forc}^{(2)}$ for structural systems reinforced by CNTs decrease. Otherwise, with the increase of external excitation P_0, the influence of FG-O profile on $\vartheta_{Forc}^{(1)}$ and $\vartheta_{Forc}^{(2)}$ decreases significantly for small values of $\bar{\theta}$, while this significance disappears as the P_0 increases. The effect of FG-X profile on $\vartheta_{Forc}^{(1)}$ and $\vartheta_{Forc}^{(2)}$ increases significantly for small values of $\bar{\theta}$, as P_0 increases, but this significance disappears, as P_0 increases.

The distributions of ratios $\vartheta_{Forc}^{(i)}/\Omega_0$ (i = 1,2) and Ω_{NL}/Ω_0 for FG-V and FG-X patterned structural systems according to $\bar{\theta}$ for fixed data $V_{cnt}^* = 0.12,\ r_1/a = 2, a/b = 1$ with various external excitation P_0 are plotted in Fig. 8. Considering these data, the ratios $\vartheta_{Forc}^{(1)}/\Omega_0$ and Ω_{NL}/Ω_0 of FG-V and FG-X profile increase while the $\vartheta_{Forc}^{(2)}/\Omega_0$ decrease with the increasing of P_0 for fixed $\bar{\theta}$. The ratio $\vartheta_{Forc}^{(1)}/\Omega_0$ of the

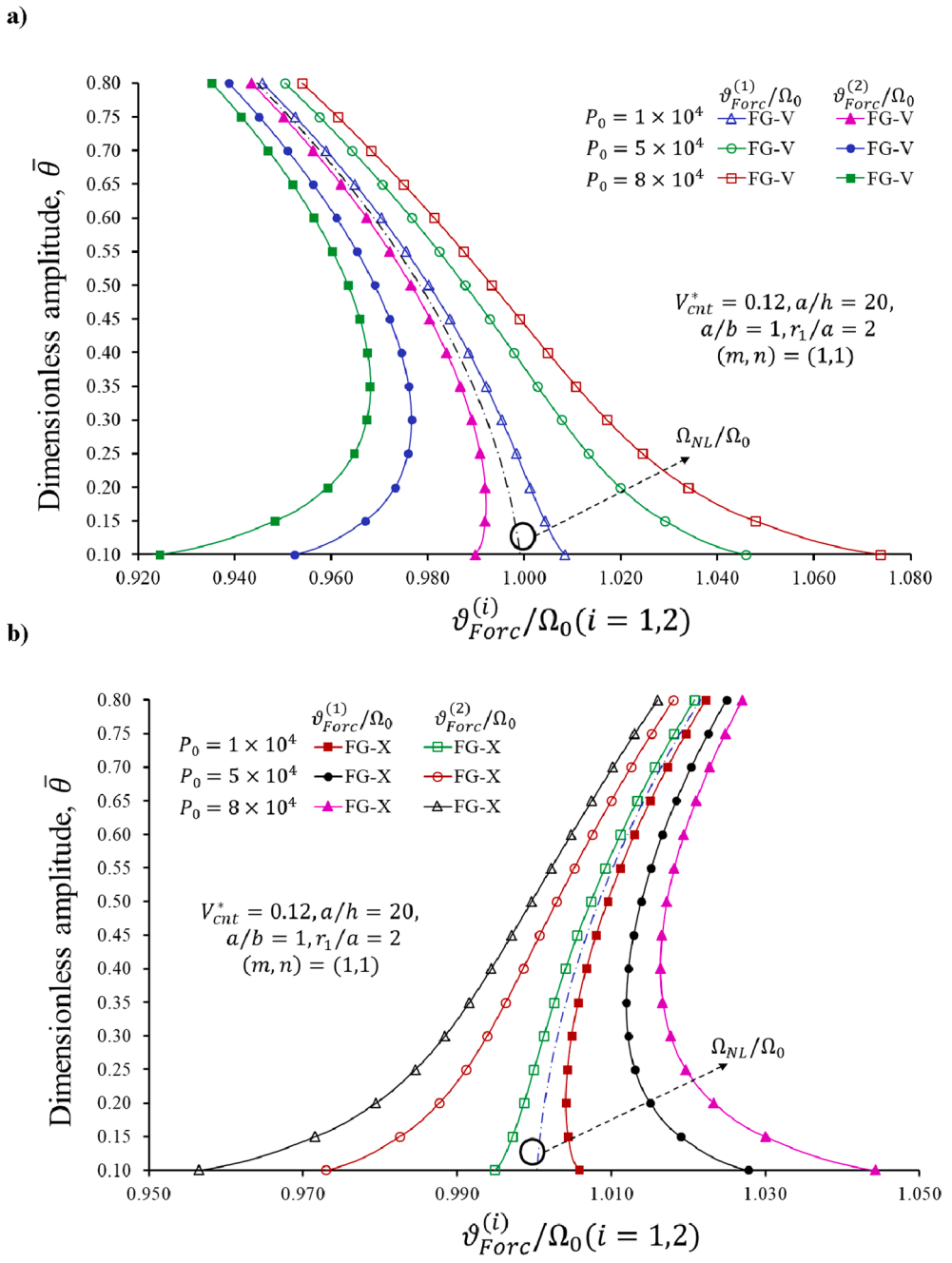

Fig. 8. Distribution of $\vartheta^{(i)}_{Forc}/\Omega_0$ (i = 1,2) and Ω_{NL}/Ω_0 for a) FG-V and b) FG-X patterned structural systems according to $\bar{\theta}$ with different external excitation P_0.

FG-V profile is greater than that of FG-X profile, while $\vartheta^{(2)}_{Forc}/\Omega_0$ is smaller for all values of P_0. The $\vartheta^{(1)}_{Forc}/\Omega_0$ $(i = 1,2)$ ratio for FG-V profile decreases continuously, while the $\vartheta^{(2)}_{Forc}/\Omega_0$ ratio increases first and then decreases as a parabolic curve by taking the maximum value, as the $\bar{\theta}$ increases. The ratios $\vartheta^{(1)}_{Forc}/\Omega_0$ and $\vartheta^{(2)}_{Forc}/\Omega_0$ for FG-X pattern increase due to increase of $\bar{\theta}$, although they are weak, for $P_0 = 10^4$(Pa). The ratio $\vartheta^{(1)}_{Forc}/\Omega_0$ first decreases and takes the minimum value and then increases in the form of a parabolic curve, while the ratio $\vartheta^{(2)}_{Forc}/\Omega_0$ continuously increase for $P_0 = 5 \times 10^4$ and 8×10^4 (Pa).

The distribution of $\vartheta^{(i)}_{Forc}/\Omega_0$ and Ω_{NL}/Ω_0 for UD and FG-V- patterned structural systems according to the $\bar{\theta}$ for fixed $V^*_{cnt} = 0.12,\ a/h = 20,\ a/b = 1$ and for different r_1/a is presented in Fig. 9. The $\vartheta^{(1)}_{Forc}/\Omega_0$ ratio of UD and FG-V patterns decreases for $r_1/a = 1$ and 2,

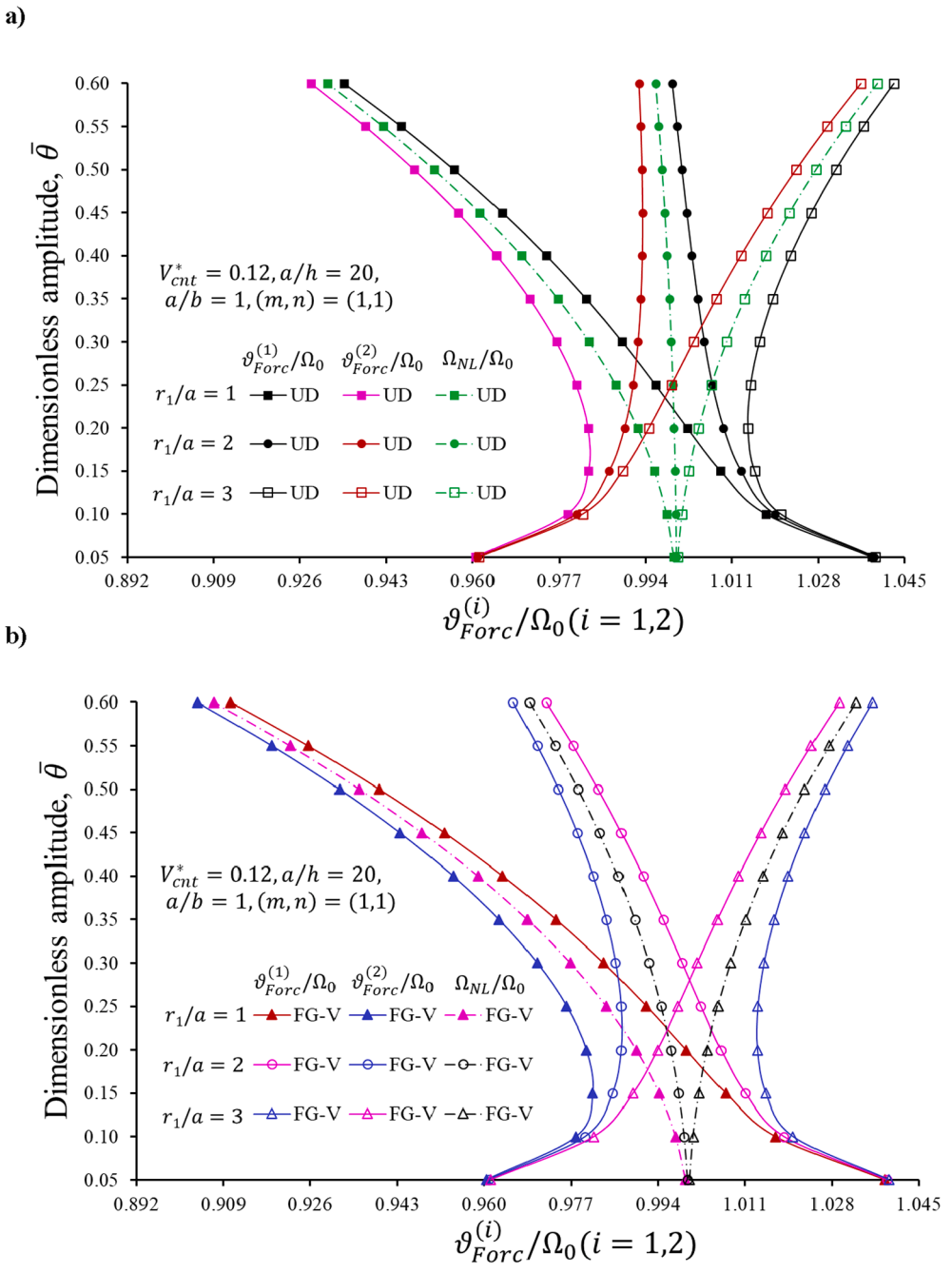

Fig. 9. Distribution of $\vartheta^{(i)}_{Forc}/\Omega_0$ (i = 1,2) and Ω_{NL}/Ω_0 for a) UD and b) FG-V patterned structural systems according to $\bar{\theta}$ for different r_1/a.

while this ratio decreases first and then takes a minimum value and increase due to the increase of the $\bar{\theta}$ for $r_1/a = 3$. The ratios $\vartheta^{(2)}_{Forc}/\Omega_0$ and Ω_{NL}/Ω_0 of UD and FG-V patterns first increase and then decrease for $r_1/a = 1$ and 2, while those increase continuously for $r_1/a = 3$ due to the increase of the $\bar{\theta}$.

The distribution nonlinear forced vibration frequenices of spherical shells containing CNTs depending on the dimensionless amplitude parameter $\bar{\theta}$ with different viscous damping coefficient ($\xi = 0.005, 0.03, 0.05, 0.08$) are presented in Fig. 10. UD and FG-O patterns are considered and other parameters are as follows: $V^*_{cnt} = 0.17$, $r_1/a = 1$, $a/b = 1$, $a/h = 20$ and $A_{P_0} = 0.048$. Fig. 10 shows that taking into account the viscous dumping leads to a decrease of $\vartheta^{(1)}_{Forc}$ values, while it supports an increase of $\vartheta^{(2)}_{Forc}$ values. The influences of viscos damping on $\vartheta^{(1)}_{Forc}$ and $\vartheta^{(2)}_{Forc}$ become more pronounced with increasing ξ, and also the viscos damping effect on $\vartheta^{(2)}_{Forc}$ is more pronounced than $\vartheta^{(1)}_{Forc}$ for the FG-O pattern. It is observed that the influence of viscos damping on nonlinear forced vibration

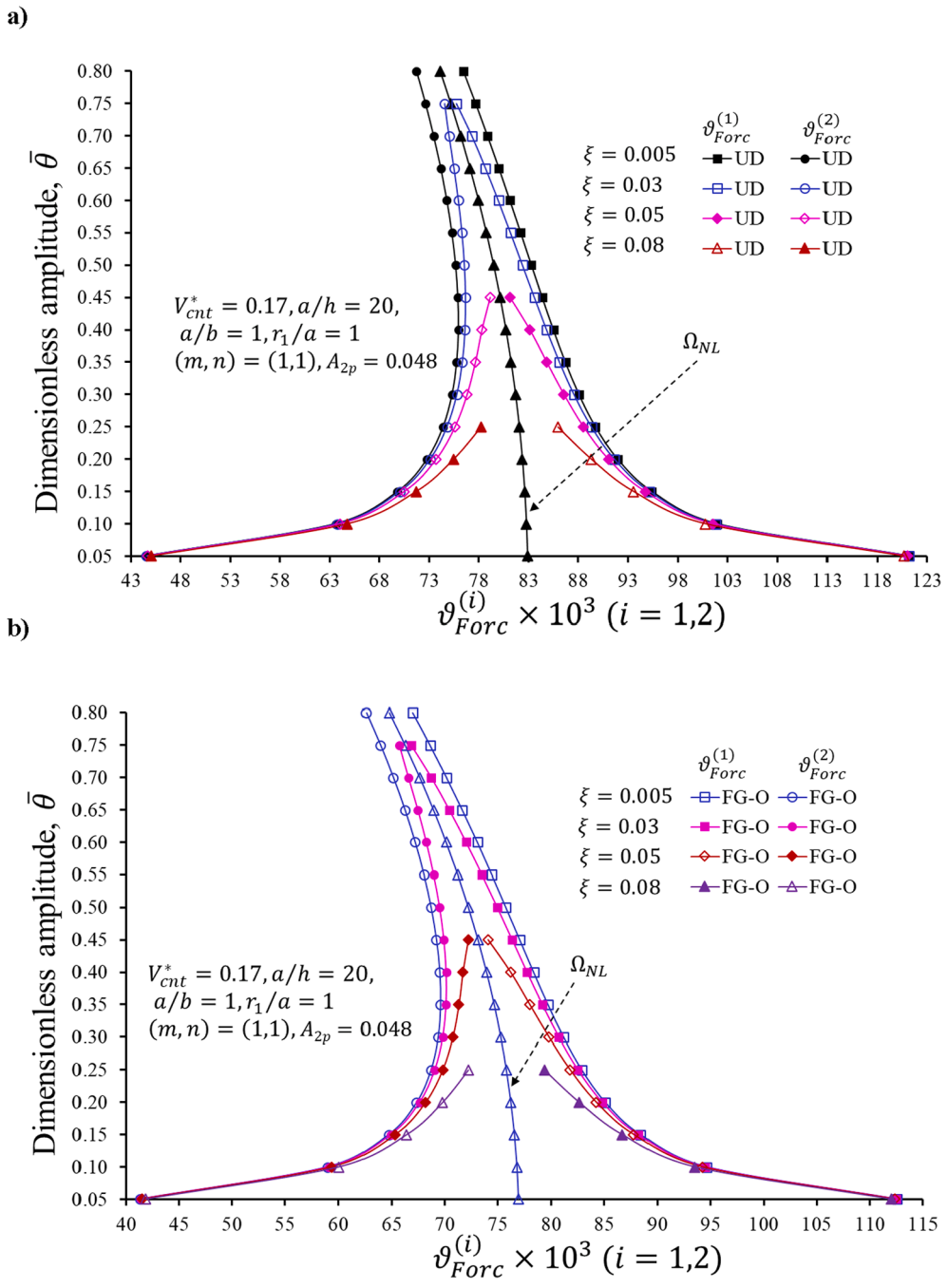

Fig. 10. Distribution of $\vartheta_{Forc}^{(i)}/\Omega_0$ (i = 1,2) for UD and FG-O patterned structural systems according to $\bar{\theta}$ with different viscous damping coefficient ξ

frequencies becomes more pronounced with the increasing of $\bar{\theta}$ for both UD and FG-O patterns. For example, the viscos damping effects on $\vartheta_{Forc}^{(1)}$ increase from (−0.06%) to (−0.45%), from (−0.18%) to (−1.34%) and from (−0.47%) to (−4.26%) for $\xi = 0.03$, 0.05 and 0.08, respectively, when $\bar{\theta}$ increases from 0.05 to 0.25. The viscos damping effects on the $\vartheta_{Forc}^{(2)}$ increase from (+0.18%) to (+0.54%), from (+0.50%) to (+1.62%) and from (+1.29%) to (+5.14%) for $\xi = 0.03$, 0.05 and 0.08, respectively, when $\bar{\theta}$ increases from 0.05 to 0.25.

5. Conclusions

In this study, the nonlinear forced vibration of structural systems reinforced by CNTs in the presence of linear viscous damping is

investigated. Hamilton principle and von Kármán-type nonlinear theory are used to obtain the nonlinear mathematical model of structural systems with the CNT pattern. To solve the non-linear problem of forced vibrations of structural systems reinforced by CNTs using Galerkin and multi-scales methods, as well as to create a dependence of nonlinear frequency on the amplitude.

Numerical analysis led to the following generalized results:

a) The influences of nonuniform patterns on $\vartheta_{Forc}^{(1)}$ and $\vartheta_{Forc}^{(2)}$ increase due to the increase of $\overline{\theta}$ and the highest influence of the pattern occurs in FG-X patterned structural systems.
b) The magnitudes of $\vartheta_{Forc}^{(1)}$ of FG-V patterned structural systems for $r_1/a = 2$ change similarly to those of $r_1/a = 1$, whereas the magnitudes of $\vartheta_{Forc}^{(1)}$ of FG-X patterned structural systems for $r_1/a = 2$ change similarly to the $r_1/a = 3$.
c) The increase of a/b significantly reduces the influence of the FG-X pattern on the magnitudes of DNFVFs.
d) With the increase of external excitation P_0, the influence of FG-O pattern on $\vartheta_{Forc}^{(1)}$ and $\vartheta_{Forc}^{(2)}$ decreases significantly for small values of $\overline{\theta}$, while this significance disappears, as the P_0 increases.
e) The influence of FG-X pattern on $\vartheta_{Forc}^{(1)}$ and $\vartheta_{Forc}^{(2)}$ increases significantly for small values of $\overline{\theta}$, as P_0 increases, but this significance disappears, when P_0 increases.
f) The ratio $\vartheta_{Forc}^{(1)}/\Omega_0$ $(i = 1,2)$ for FG-V patterned structural systems decreases continuously, while the ratio $\vartheta_{Forc}^{(2)}/\Omega_0$ increases first and then decreases as a parabolic curve by taking the maximum value, as $\overline{\theta}$ increases.
g) The influences of viscos damping on $\vartheta_{Forc}^{(1)}$ and $\vartheta_{Forc}^{(2)}$ become more pronounced with increasing ξ, and also the influence of viscos damping on $\vartheta_{Forc}^{(2)}$ is more pronounced than $\vartheta_{Forc}^{(1)}$.
h) The influence of viscos damping on the nonlinear forced vibration frequency becomes more pronounced with the increasing of $\overline{\theta}$ for both UD and FG-O patterns.

CRediT authorship contribution statement

A.H. Sofiyev: Formal analysis, Investigation, Writing - original draft. **M. Avey:** Conceptualization, Methodology, Funding acquisition, Formal analysis, Writing - review & editing. **N. Kuruoglu:** Writing - review & editing.

Declaration of Competing Interest

The authors declare that they have no known competing financial interests or personal relationships that could have appeared to influence the work reported in this paper.

References

[1] S. Iijima, Helical microtubules of graphitic carbon, Nature 354 (1998) 56–58.
[2] M.S.P. Shaffer, A.H. Windle, Fabrication and characterization of carbon nanotube/poly (vinyl alcohol) composites, Adv. Mater. 11 (11) (1999) 937–941.
[3] J. Silvestre, N. Silvestre, J. de Brito, Polymer nanocomposites for structural applications: Recent trends and new perspectives, Mech. Adv. Mater. Struct. 23 (11) (2016) 1263–1277.
[4] P.M. Ajayan, O. Stephan, C. Colliex, D. Trauth, Aligned carbon nanotube arrays formed by cutting a polymer resin-nanotube composite, Science 265 (1994) 1212–1214.
[5] L. Jin, C. Bower, O. Zhou, Alignment of carbon nanotube in a polymer matrix by mechanical stretching, Appl. Phys. Lett. 73 (9) (1998), 1197-1193.
[6] M. Baibarac, P. Gomez-Romero, Nanocomposites based on conducting polymers and carbon nanotubes from fancy materials to functional applications, J. Nanosci. Nanotechn. 6 (1) (2006) 1–14.
[7] M. Moniruzzaman, K.I. Winey, Polymer nanocomposites containing carbon nanotubes, Macromolecules 39 (2006) 5194–5205.
[8] S. Bal, S.S. Samal, Carbon nanotube reinforced polymer composites, A State of the Art, Bull. Mater. Sci. 30 (4) (2007) 379–386.
[9] A. Al-Ostaz, G. Pal, P.R. Mantena, A. Cheng, Molecular dynamics simulation of SWCNT-polymer nanocomposite and its constituents, J. Mater. Sci. 43 (2008) 164–173.
[10] W. Wang, P. Ciselli, E. Kuznetsov, T. Peijs, A.H. Barber, Effective reinforcement in carbon nanotube-polymer composites, Phil. Trans. Math. Phys. Eng. Sci. 366 (2008) 1613–1626.
[11] J.N. Ginsberg, Large amplitude forced vibrations of simply supported thin cylindrical shells, J. Appl. Mech. 40 (1973) 471–477.
[12] D. Hui, Influence of geometric imperfections and in-plane constraints on nonlinear vibrations of simply supported cylindrical panels, J. Appl. Mech. 51 (2) (1984) 383–390.
[13] K. Yasuda, G. Kushida, Nonlinear forced oscillations of a shallow spherical shell, Bull. Jpn. Soc. Mech. Eng. 27 (1984) 2233–2240.
[14] N.S. Bardell, J.M. Dunsdon, R.S. Langley, Free and forced vibration analysis of thin, laminated, cylindrically curved panels, Compos. Struct. 38 (1) (2008) 453–462.
[15] F. Pellicano, M. Amabili, M.P. Paıdoussis, Effect of the geometry on the non-linear vibration of circular cylindrical shells, Int. J. Non-Lin. Mech. 37 (2002) 1181–1198.
[16] K.V. Avramov, Nonlinear forced vibrations of a cylindrical shell with two internal resonances, Int. Appl. Mech. 42 (2) (2006) 169–175.
[17] M. Rougui, F. Moussaoui, R. Benamar, Geometrically non-linear free and forced vibrations of simply supported circular cylindrical shells: a semi-analytical approach, Int. J. Non-Lin. Mech. 42 (2007) 1102–1115.
[18] G. Pilgun, M. Amabili, Analysis of nonlinear forced vibrations of shallow shells with cut-outs by using the r-function method, ASME, Int. Mech. Eng. Congress. Expos. (2011) 783–792.
[19] H.L. Dai, H.J. Jiang, Forced vibration analysis for a FGPM cylindrical shell, Shock Vib. 20 (3) (2013) 531–550.
[20] J.G.N. Zenon del Prado, A.L.D.P. Argenta, F.M.A. da Silva, P.B. Gonçalves, The effect of material and geometry on the non-linear vibrations of orthotropic circular cylindrical shells, Int. J. Non-Lin. Mech. 66 (2014) 75–86.
[21] C. Du, Y. Li, X. Jin, Nonlinear forced vibration of functionally graded cylindrical thin shells, Thin-Wall. Struct. 78 (2014) 26–36.

[22] J. Plattenburg, J.T. Dreyer, R. Singh, A new analytical model for vibration of a cylindrical shell and cardboard liner with focus on interfacial distributed damping, Mech. Syst. Signal Process. 75 (2016) 176–195.
[23] G.G. Sheng, X. Wang, The non-linear vibrations of rotating functionally graded cylindrical shells, Nonlin. Dyn. 87 (2017) 1095–1109.
[24] G.G. Sheng, X. Wang, G. Fu, H. Hu, The nonlinear vibrations of functionally graded cylindrical shells surrounded by an elastic foundation, Nonlin. Dyn. 78 (2014) 1421–1434.
[25] G.G. Sheng, X. Wang, Nonlinear vibrations of FG cylindrical shells subjected to parametric and external excitations, Compos. Struct. 191 (2018) 78–88.
[26] G.G. Sheng, X. Wang, The dynamic stability and nonlinear vibration analysis of stiffened functionally graded cylindrical shells, Appl. Math. Model. 56 (2018) 389–403.
[27] Q. Dai, Q. Cao, Parametric instability analysis of truncated conical shells using the Haar wavelet method, Mech. Syst. Signal Process. 105 (2018) 200–213.
[28] H. Arvin, A. Arena, W. Lacarbonara, Nonlinear vibration analysis of rotating beams undergoing parametric instability: Lagging-axial motion, Mech. Syst. Signal Process. 144 (2020), 106892.
[29] J.F. Wang, J.P. Yang, L.H. Tam, W. Zhang, Molecular dynamics-based multiscale nonlinear vibrations of PMMA/CNT composite plates, Mech. Syst. Signal Process. 153 (2021), 107530.
[30] M. Amabili, P. Balasubramanian, Nonlinear forced vibrations of laminated composite conical shells by using a refined shear deformation theory, Compos. Struct. 249 (2020), 112522.
[31] S. Suresh, A. Mortensen, Fundamentals of Functionally Graded Materials: Processing and Thermomechanical Behavior of Graded Metals and Metal-Ceramic Composites, IOM Communications Ltd, London, 1998.
[32] H.S. Shen, Nonlinear bending of functionally graded carbon nanotube-reinforced composite plates in thermal environments, Compos. Struct. 91 (1) (2009) 9–19.
[33] H.S. Shen, Y. Xiang, Nonlinear vibration of nanotube-reinforced composite cylindrical shells in thermal environments, Comp. Meth. Appl. Mech. Eng. 213 (2012) 196–205.
[34] H.S. Shen, D.Q. Yang, Nonlinear vibration of functionally graded fiber-reinforced composite laminated cylindrical shells in hygrothermal environments, Appl. Math. Model. 39 (2015) 1480–1499.
[35] N.D. Duc, T.Q. Quan, V.D. Luat, Nonlinear dynamic analysis and vibration of shear deformable piezoelectric FGM double curved shallow shells under damping-thermo-electro-mechanical loads, J Compos. Struct. 125 (2015) 29–40.
[36] H.S. Shen, X.Q. He, Large amplitude free vibration of nanotube-reinforced composite doubly curved panels resting on elastic foundations in thermal environments, J. Vib. Control 23 (16) (2017) 2672–2689.
[37] N.D. Duc, J. Lee, T.T. Nguyen, P.T. Thang, Static response and free vibration of functionally graded carbon nanotube-reinforced composite rectangular plates resting on Winkler-Pasternak elastic foundations, J. Aerospace Sci. Techno. 68 (2017) 391–402.
[38] N.V. Thanh, N.D. Khoa, N.D. Tuan, P. Tran, N.D. Duc, Nonlinear dynamic response and vibration of functionally graded carbon nanotubes reinforced composite (FG-CNTRC) shear deformable plates with temperature dependence material properties and surrounded on elastic foundations, J. Therm. Stress. 40 (10) (2017) 1254–12749.
[39] N.D. Khoa, V.M. Anh, N.D. Duc, Nonlinear dynamic response and vibration of functionally graded nanocomposite cylindrical panel reinforced by carbon nanotubes in thermal environment, J. Sand. Struct. Mater. (2019), https://doi.org/10.1177/109963 6219 84 7191.
[40] K. Foroutan, H. Ahmadi, E. Carrera, Nonlinear vibration of imperfect FG-CNTRC cylindrical panels under external pressure in the thermal environment, Compos. Struct. 2271 (2019), 111319.
[41] M. Amir, M. Talha, Nonlinear vibration characteristics of shear deformable functionally graded curved panels with porosity including temperature effects, Int. J. Pres. Ves. Pip. 172 (2019) 28–41.
[42] S.S. Tomar, M. Talha, Large amplitude vibration analysis of functionally graded laminated skew plates in thermal environment, Mech. Adv. Mater. Struct. 26 (5) (2019) 451–464.
[43] H.S. Shen, C. Li, J.N. Reddy, Large amplitude vibration of FG-CNTRC laminated cylindrical shells with negative Poisson's ratio, Comp. Meth. Appl. Mech. Eng. 360 (2020), 112727.
[44] J. Yang, X.H. Huang, H.S. Shen, Nonlinear vibration of temperature-dependent FG-CNTRC laminated plates with negative Poisson's ratio, Thin-Wall. Struct. 148 (2020), 106514.
[45] N.D. Dat, N.V. Thanh, V.M. Anh, N.D. Duc, Vibration and nonlinear dynamic analysis of sandwich FG-CNTRC plate with porous core layer, J Mech. Adv. Mater. Struct. (2020), https://doi.org/10.1080/15376494.2020.1822476.
[46] D.T. Manh, V.T.T. Anh, P.D. Nguyen, N.D. Duc, Nonlinear post-buckling of CNTs reinforced sandwich-structured composite annular spherical shells, Int. J. Struct. Stab. Dyn. (2020), https://doi.org/10.1142/S0219455420500182.
[47] H.M. Sedighi, M. Malikan, Stress-driven nonlocal elasticity for nonlinear vibration characteristics of carbon/boron-nitride hetero-nanotube subject to magneto-thermal environment, Phys. Scrip. 95 (5) (2020), 055218.
[48] N.D. Dat, T.Q. Quan, N.D., Duc Nonlinear thermal vibration of carbon nanotube polymer composite elliptical cylindrical shells, Int. J. Mech. Mater. Des. 16 (2) (2020) 331–350.
[49] B. Zhu, Q. Xu, M. Li, Y. Li, Nonlinear free and forced vibrations of porous functionally graded pipes conveying fluid and resting on nonlinear elastic foundation, Compos. Struct. 252 (2020), 112672.
[50] S. Zghal, A. Frikha, F. Dammak, Large deflection responses-based geometrical nonlinearity of nanocomposite structures reinforced with carbon nanotubes, Appl. Math. Mech.-Engl. Ed. 41 (2020) 1227–1250.
[51] E. Mahmure, Avey Yusufoglu, On the solution of large-amplitude vibration of carbon nanotube-based doubly-curved shallow shells, Math. Meth. Appl. Sci. (2020) 1–12 (in press).
[52] A.S. Volmir, The Nonlinear dynamics of plates and shells, Moscow: Sci. Edit. (1972).
[53] N.D. Duc, Nonlinear Static and Dynamic Stability of Functionally Graded Plates and Shells, Vietnam Nat. Uni. Press, Hanoi, 2014.
[54] Z.M. Pekerman, K.Z. Galimov, On large deflections of orthotropic panels rectangular in plan-view, Stud. Theory Plate. Shell. 1 (9) (1972) 228–246.
[55] A.H. Nayfeh, D.T. Mook, Nonlinear Oscillations, Wiley, New York, 1979.
[56] B.A. Selim, L.W. Zhang, K.M. Liew, Vibration analysis of CNT reinforced functionally graded composite plates in a thermal environment based on Reddy's higher-order shear deformation theory, Compos. Struct. 156 (2016) 276–290.